Materials Research Proceedings 44 (2024) 167-181 https://doi.org/10.21741/9781644903254-19

Surface integrity analysis of 304 stainless steel after slurry blasting

CHAI Ze-lin[1], ZHOU Cun-long[1*], GUO Rui[1] and JIANG Zhengyi[2]

[1]Shanxi Provincial Key Laboratory of Metallurgical Equipment Design and Technology, College of Mechanical Engineering, Taiyuan University of Science and Technology, Taiyuan 030024, China

[2] TYUT-UOW Joint Research Center, University of Wollongong, Wollongong, NSW 2522, Australia

zcunlong@tyust.edu.cn

Keywords: Slurry Blasting, Surface Integrity, Surface Roughness, Residual Stress, Corrosion Resistance

Abstract. The Eco Pickled Surface technology has attracted increasing attention due to its green and environmentally friendly characteristics. However, due to the complex internal structure of the oxide skin and the diverse bonding methods with the substrate surface, as well as the failure to establish a relationship between the substrate surface integrity and process parameters after descaling, the widespread application of this technology is restricted. The 304 stainless steel hot-rolled plates and strips had been researched in this article, and the finite element ANSYS/AUTODYN modules had been used to simulate the descaling process; An analysis was conducted on the surface integrity of 304 stainless steel after descaling, including roughness, residual stress, and corrosion resistance. The results showed that: The maximum temperature on the substrate surface under different abrasive particle sizes, blasting speeds, and blasting angles is 95℃;the impact range and depth of the substrate surface after slurry blast will increase with the increase of abrasive particle size and injection speed, The maximum hardened layer after slurry impact is 140 μm; The minimum corrosion current density on the substrate surface after slurry impact can reach 1.29*10-6A/cm2, the corrosion resistance of the substrate surface has been significantly improved, and the EBSD results show that the grains after slurry impact are concentrated in 4-19 μm, maximum 22 μm. The average grain size is 10.79 μm.

Introduction

The slurry descaling technology represented by EPS technology has attracted increasing interest and attention due to its green and environmentally friendly characteristics [1]. However, due to the diverse types and complex structures of oxide scales on metal surfaces of different materials, as well as the lack of sufficient critical strain data for oxide scale rupture, it is difficult to establish a comprehensive slurry impact process model, resulting in difficulty in controlling the surface integrity after descaling. With the advancement of technology, people have higher requirements for the surface roughness, residual stress, and corrosion resistance of plates and strips after leaving the factory. However, due to the lack of relationship between surface integrity and process parameters, the promotion of this technology is greatly affected. Among them, the impact energy of the slurry determined by the coupling of various process parameters directly affects the cracking and peeling of the oxide scale and the elastic-plastic deformation of the substrate surface. Therefore, analyzing the relationship between the impact energy of the slurry during the slurry throwing process and the integrity of the substrate surface after descaling is of great significance for the slurry throwing descaling process.

Finnie [2] assumes that when the abrasive particles of a rigid body impact elastic-plastic metal materials, the deformation follows the three-dimensional grinding theory, which involves three stages: sliding, plowing, and cutting. A material removal volume expression related to abrasive

particle size and impact angle was established based on the chip volume generated by the abrasive particles within the operating distance. When the deformation is small, it is based on the theory of elastic-plastic deformation. Bitter [3] assumes that the abrasive particles of an elastic body impact elastic-plastic materials in two directions of motion, namely the direction perpendicular to the surface of the workpiece and the direction parallel to the workpiece. According to Hertz theory, the vertical direction is used to obtain the impact force, the diameter and depth of the impact crater, and thus establish a material deformation model; The horizontal direction is calculated based on the energy required to convert abrasive kinetic energy into shear volume. On this basis, Zhang Chengguang et al. used Hertz's law to incorporate the shape of abrasives in actual production and the elastic deformation of pits after impact into the material deformation model, making the predicted results closer to reality [4]. The Duan team conducted an experiment on the impact of abrasive impact on the microstructure of hot-dip galvanized steel layers. By measuring the morphology, roughness, residual stress, phase composition, and hardness of the samples, the impact of abrasive impact on the steel matrix was evaluated. The experimental results showed that after abrasive impact, the rigid matrix exhibited severe plastic deformation, and the tensile stress on the surface transformed into compressive residual stress. The surface roughness and hardness were greatly improved, The compression residual stress suppresses the dissolution of Fe atoms, resulting in a thinner coating. The refinement of grains and the generation of grain defects promote the diffusion of Fe and Zn in the early stage of the reaction, shorten the reaction time, and thus increase the coating thickness. The thickness of the entire coating of the sample decreases with the increase of surface roughness [5]. Some studies consider the deformation of metal surface contours, which is caused by the elastic-plastic deformation of the contour peaks being flattened, resulting in changes in the roughness of the metal surface [6]. Reference [7] indicates that when the abrasive particle size is optimal, the surface roughness Ra of the substrate after descaling can reach the quality level of high-quality acid washed boards (Ra1.6). Due to the fact that the deformation heat of the workpiece is rapidly carried away by the fluid during the impact process of abrasive slurry, and the surface roughness can reach very small, this technology has been widely applied in the polishing and precision grinding of ultra precision optical components, superhard materials Si3N4 and Al2O3 in recent years. The surface roughness of the processed workpiece reaches the nanometer level [8]. Vedansh Chaturvedi [9] conducted experimental research on the impact of abrasive slurry on 304 stainless steel plates, established an optimization model with lateral velocity, target distance, abrasive flow rate, and water pressure as optimization parameters, and surface roughness as the objective function, and optimized the parameters using sound to noise ratio technology. Sudhakar R studied the effects of abrasive particle size and velocity, nozzle lateral velocity, and target distance on surface roughness, and fitted the corresponding relationship between abrasive particle motion parameters and roughness values [10]. Scholars such as Benjamin Levy, Mohammed EI Mansori, and Mourad El Hadrouz have studied the impact of slurry abrasives on surface substrates through the concept of digital twins. They have captured abrasive trajectories using high-speed cameras and measured abrasive flow rates using flow sensors to fit the effects of abrasive particle size, density, and environmental pressure on substrate surface roughness. They have also proposed the concept of EASR, which only analyzes representative surfaces and no longer requires complete three-dimensional shape measurements of the entire surface, The use of EASR can effectively describe the characteristics of the substrate surface to create numerical models and optimize econometric characterization [11]. Scholars such as Navdeep Minhas, Ankit Thakur, Sumit Mehlwal, and others conducted experimental research on the surface treatment of AlSi10Mg alloy by slurry treatment. Three input parameters (slurry time, abrasive velocity, and abrasive particle size) were selected at three levels to set the matrix, and a quadratic model was established using response surface methodology. The experimental results showed that abrasive velocity had the greatest impact on surface roughness, with a positive

effect (41.89%), followed by slurry time (29.29%) and abrasive particle size (23.71%) The negative impact is significant, and the predicted surface roughness values (maximum and minimum values) obtained under the optimal process parameters are consistent with the experimental measurement values (± 6%) [12]. The grain structure and mechanical properties will undergo changes after abrasive impact on the metal surface. The Yang Fan team from Tongji University conducted a random shot blasting experiment, and the results showed that residual compressive stress is a beneficial side effect of abrasive removal of metal surface oxide skin. It can effectively delay crack propagation, significantly extend the fatigue life of working parts, and establish the relationship between maximum residual stress and compressive stress depth with abrasive speed, impact angle, and abrasive particle size by developing ABAQUS/Python scripts, The impact angle is the largest influencing factor [13]. Moonchaleanporn, Pongporn, Sukrit Songkuea and other scholars conducted corrosion resistance experiments on 304L stainless steel abrasive under different sintering gas conditions. 304L stainless steel was sintered at two different heating rates under nitrogen and argon gas, and then subjected to abrasive impact. Subsequently, salt spray tests were conducted on the samples to determine their corrosion resistance; The experimental results show that the surface porosity and roughness of the shot material have significantly changed after impact, and the surface hardness has significantly increased. The corrosion resistance of 304L sintered under argon gas conditions is significantly higher than that under nitrogen gas conditions, and there is no strong theoretical support for the reasons for the differences [14]. Scholars such as Gurmider Singh and Gurmider Singh conducted abrasive impact tests on the surface of AZ31 alloy. After analyzing the factors affecting surface roughness, material removal rate, and corrosion resistance, they first proposed that abrasive impact on the surface of AZ31 alloy can improve metal biological activity. After abrasive impact, the rough surface provides strong mechanical locking for the initial stage of cell adhesion, resulting in good cell growth characteristics, Therefore, abrasive impact surfaces can also be applied in the medical industry [15]. The grains on the surface of the metal are refined and the microstructure becomes compact. The residual stress introduced after impact strengthens the metal surface, increases hardness, and at the same time, the yield limit and strength limit of the metal surface are also improved. The corrosion resistance of the rolled piece is correspondingly increased, and the service performance is also improved [16]. However, the relationship between corrosion resistance and the kinetic parameters of abrasive particles is still in the qualitative stage.

In recent years, our research group has studied the influence of jet process parameters on material surface pressure and roughness [17-18], but the impact of abrasive particle impact on substrate surface roughness and corrosion resistance is still in the experimental stage.

In summary, research on the mechanism of action of slurry on the substrate surface and its impact on corrosion resistance is still in the process of regular exploration and has not yet formed a systematic theoretical system, lacking theoretical guidance for regulating surface quality and performance. Therefore, this article intends to take 304 stainless steel as the research object, and reveal the synergistic mechanism of different process parameters on the surface roughness and corrosion resistance of the substrate by studying the deformation law and characteristics of the microstructure of the substrate material and its influence on the mechanical properties such as work hardening and residual stress, in order to achieve flexible control of the surface quality of the substrate; Ultimately, it provides theoretical and technical basis for the systematic study of the deformation mechanism of abrasive impact on metal surfaces, solving the optimization problem of various process parameters in acid free descaling process, and developing new technologies, devices, and processes for removing oxide scales.

Analysis of the impact mechanism of slurry blasting

T In the slurry blasting process, the slurry enters the blade of the blast machine from the blasting chamber and is accelerated under centrifugal force. Afterward, the slurry leaves the blade at a

certain angle and generates a total impact force (F) on the oxide scale of the metal matrix surface. The vertical component is the impact force F1, and the horizontal component is the micro-cutting force F2, as shown in Fig. 1. Some studies have shown that the slurry blasting impact is a high-angle projectile greater than 50° with circular abrasive particles. Therefore, the effect of slurry blasting impact on the abrasive particles is dominant, while the horizontal micro-cutting effect is not significant[19-21]. After the oxide skin ruptures and peels off under external loads, the impact energy of abrasive particles will act on the surface of the substrate, causing elastic-plastic deformation of the substrate, thereby affecting the integrity of the substrate surface.

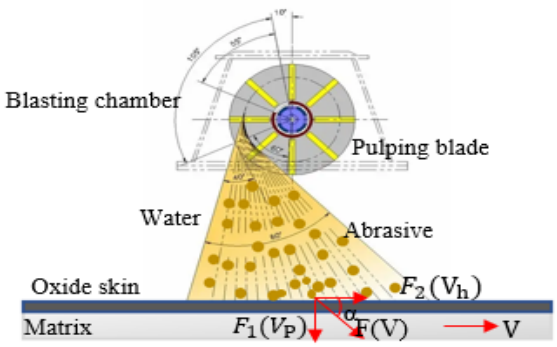

Fig. 1. Schematic diagram of slurry impact force.

Finite element analysis of slurry blasting

In order to analyze the surface quality of the substrate after slurry impact from an energy perspective, the finite element simulation analysis of the slurry process will be conducted below.

Establishment of finite element model. The finite element analysis was conducted using the ANSYS/AUTODYN module, while the AUTODYN modeling was carried out using the SPH method. The SPH method discretizes a fluid or solid into a series of particles that move without any connecting action, each particle being an independent interpolation point. By using specific calculation methods to combine the mechanical properties of each particle, it achieves an overall approximation of the actual mechanical properties of the modeled object [22].

In the slurry impact, the slurry is selected as a mixture of water and abrasive particles. The slurry in the slurry is a mixture model of water and abrasive particles, with a total of 20024 SPH particle units. The model parameters are shown in Table 1.

Using Lagrange to establish a workpiece model, 304 was selected as the target material in the material library, and the performance parameters were not changed; The modeling size of the target is 100 mm x 100 mm x 3 mm, with a total of 515121 Lagrange particle units. The edge length of the unit at the impact point is 0.1 mm, and the rest is 0.5 mm. The finite element model is shown in Fig. 2.

Table1. Finite element model parameters.

	bulasting medium	number of particles	Angle/°	cast/mm
Slurry blasting	steel shot、water	20024	90	340

The independent variables of finite element calculation are the initial velocity of the slurry and the particle size of the abrasive. In order to reduce computational complexity, finite element analysis assumes that: (1) the materials involved in the slurry impact process include water, abrasive, and 304 workpiece. (2) Both water particles and abrasive particles are spherical. (3) Water particles are randomly distributed and their velocity is the same as the initial velocity of the abrasive. (4) The time for abrasive particles to impact the surface of the substrate is 10-5 seconds.

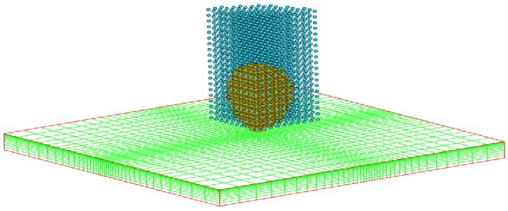

Fig. 2. Schematic diagrams of finite element model slurry blasting.

Instantaneous velocity of slurry impact on the surface of the substrate. The instantaneous velocity when the slurry impacts the surface of the substrate is shown in Fig. 3, and the abrasive particle size When the initial velocity is 80 m · s^{-1} at 1 mm, the instantaneous velocity of the abrasive particle impacting the substrate surface is 40-46 m · s^{-1}, and the velocity attenuation rate during the entire motion process is 43%~50%.

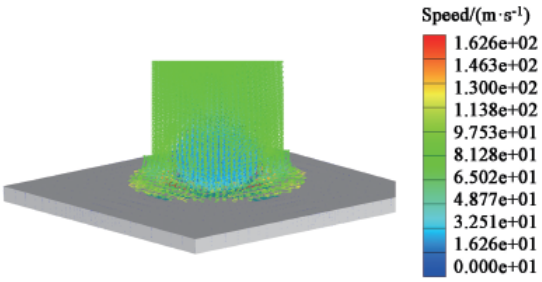

Fig. 3. Schematic diagrams of instantaneous velocity of during the impact of matrix surface by slurry blasting.

The instantaneous velocity of the slurry impacting the surface of the substrate decreases significantly. The reason for this phenomenon is that the water flow in the slurry abrasive slurry also has a higher initial velocity. When the water flow rebounds upon the substrate, a certain static pressure area is formed due to the continuity of the fluid, as shown in Figure 4. The abrasive particles are dispersed solid particles, so they can pass through the static pressure zone and impact the substrate, while the water flow will not enter this static pressure zone due to its continuity. The static pressure direction of the static pressure zone formed by the fluid is from the inside out, and the maximum static pressure value is at the center. When the initial velocity is 80 m · s^{-1}, the maximum static pressure is 69.1 kPa. When the abrasive particles pass through this area, due to the influence of static pressure resistance, the abrasive particle velocity will decrease by 43% to 50%.

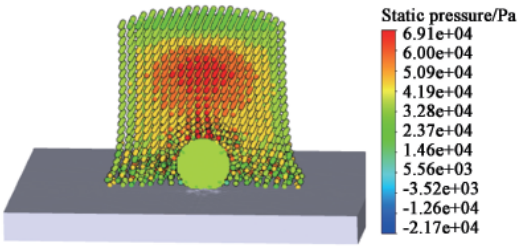

Fig. 4. Schematic diagram of static pressure zone finite element calculation.

Instantaneous velocity of slurry impact on the surface of the substrate. After slurry impact, plastic deformation occurs on the surface of the substrate, forming pits, as shown in Fig. 5. The impact depth and impact diameter of abrasive particles on the substrate have a significant impact on the surface quality of the substrate after impact. The finite element calculation results of the depth and diameter of slurry impact under different process parameters are shown in Fig. 6. The particle size of the slurry abrasive is determined by 0.6 mm increased to 1.0 mm, increase impact depth by 65%, increase impact diameter by 17%; The ejection velocity increased from 60 m · s^{-1} to 80 m · s^{-1}, the impact depth increased by 36%, and the impact diameter increased by 10%.

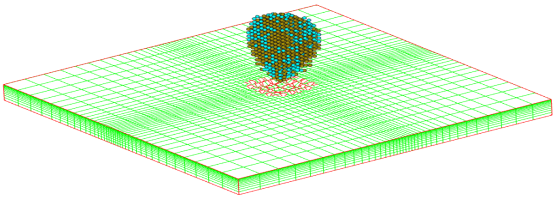

Fig. 5. Plastic deformation of matrix surface after impac.

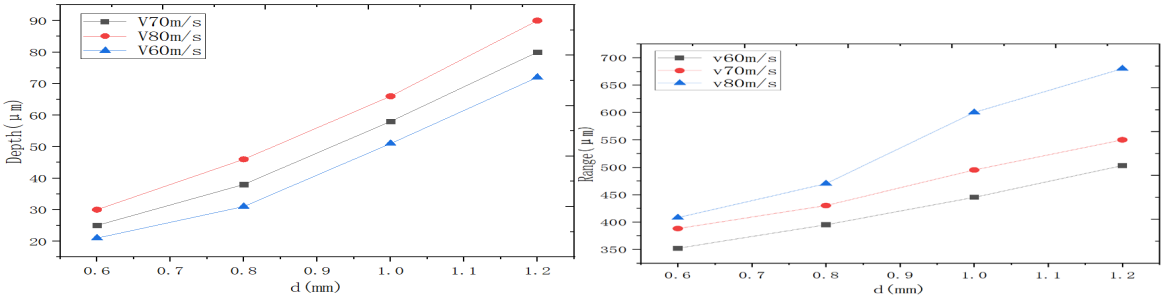

Fig. 6. impact depth（a）and impact diameter（b）of slurry blasting.

Instantaneous temperature of the substrate surface during slurry impact. The kinetic energy of abrasive particles is not only converted into impact energy on the surface of the substrate, but also a portion of the energy is converted into thermal energy due to the collision between the abrasive particles and the substrate. The collision of the two will cause an increase in the surface temperature of the substrate, while the mechanical properties of metal materials will undergo significant changes due to the increase in surface temperature. Therefore, it is necessary to analyze the thermal energy generated by the collision.

ROWE et al. [23] established a heat distribution ratio model between workpiece and abrasive particles from a microscopic perspective by studying the interaction between abrasive particles and matrix:

$$R = \left\{1 + \frac{0.97k_g}{\sqrt{r_g v_s k_w \rho_w c_w}}\right\}^{-1} \quad (1)$$

Where,k_g- the thermal conductivity of the abrasive material,r_g- the contact radius between the abrasive and the workpiece(mm), v_s- the abrasive impact velocity(m/s),k_w- the matrix thermal conductivity,ρ_w- the matrix density, c_w- the specific heat capacity of the matrix material.

Yu Zhipeng [24] established a three-dimensional temperature field equation for the collision of a single abrasive particle with a workpiece based on Eq. 1. The research results show that the collision temperature generated when the abrasive particle just contacts the surface is the highest, and the temperature generated by the collision of spherical abrasive particles is higher than that of other shapes. Therefore, when studying the instantaneous maximum temperature during shot blasting and slurry impact, the initial time of collision between the abrasive particles and the substrate should be selected. Assuming that the contact point on the surface of the workpiece is spherical, its diameter will be much smaller than the diameter of the pit, and its temperature rise will be greater than the calculated value of Eq. 1. Moreover, the energy conversion rate during instantaneous collision cannot be accurately calculated. In order to further calculate the instantaneous temperature at the beginning of the collision, finite element analysis was conducted on the temperature change during the collision process, as shown in Fig. 7.

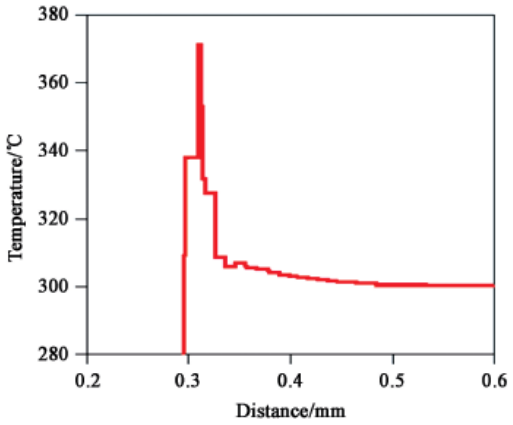

Fig .7. Finite element calculation results of temperature during abrasive impact process.

The results in Fig. 7 indicate that the center point of the collision contact has the highest temperature, and the edge gradually decreases; The center point of the slurry impact is offset due to the action of free fluid. When extracting the instantaneous temperature calculation results of finite element method under different process parameters for slurry impact, the instantaneous temperature change on the substrate surface is not significant with the change of process parameters, and the range of change is 60-97℃.

The results show that the entire process of slurry impact is significantly lower than that of shot blasting due to the instantaneous velocity during collision, and the presence of continuous fluid results in a large amount of heat generated during the entire process being carried away by high-speed water flow; Although the static pressure zone formed by continuous fluid may hinder the loss of heat to a certain extent, when discrete abrasive particles pass through the static pressure zone, they will also carry water into it. At the same time, the range of the static pressure zone formed is small, and the high-speed movement of the boundary fluid will still carry away the heat generated by the impact. Therefore, the surface temperature of the substrate will not change significantly during the entire process of slurry impact.

Experimental study on the surface integrity of 304 stainless steel substrate after slurry impact

The previous text used finite element analysis to study the mechanism of surface deformation of the substrate caused by slurry impact. In order to verify the finite element results and quantitatively analyze the integrity of the surface of 304 stainless steel after slurry impact, this paper conducted slurry impact tests on 304 stainless steel.

Test materials and methods. The slurry impact test was conducted on the self-developed slurry and slurry combined descaling experimental platform by our research group; The sample is a hot-rolled 304 stainless steel plate with surface oxide skin not removed, with dimensions of 100 mm * 100 mm * 3 mm; The abrasive grains are selected as cast steel pellets (with a Vickers hardness of 5 GPa and a density of 7.5g/cm3). The experimental parameters are shown in the Table 2.

Table 2. Experimental parameters for slurry throwing.

d	D/steel shoot	water	v(r/min)	cast	time
0.6mm	3L	4L	1600~2900	340mm	10s
0.8mm	3L	4L	1600~2900	340mm	10s
1.0mm	3L	4l	1600~2900	340mm	10s
1.2mm	3L	4L	1600~2900	340mm	10s

Analysis of Surface Roughness. The dense oxide layer on the matrix surface disappeared after the slurry impact. In addition, the plastic deformation caused by slurry impact leads to pits of different depths on the matrix surface (Fig. 8).

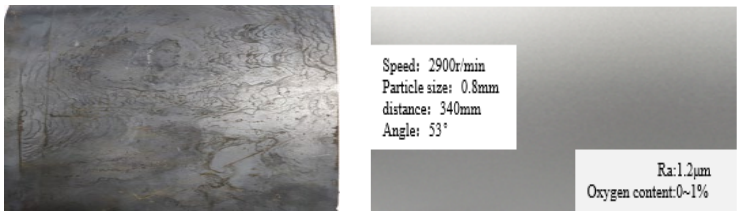

Fig. 8. Schematic diagram of 304 stainless steel after descaling for (a) 304 stainless steel sample before descaling, (b) 304 stainless steel sample after descaling.

The surface roughness after slurry impact was measured using the Mitutoyo SJ410 roughness measuring instrument, and the results are shown in Fig. 9.

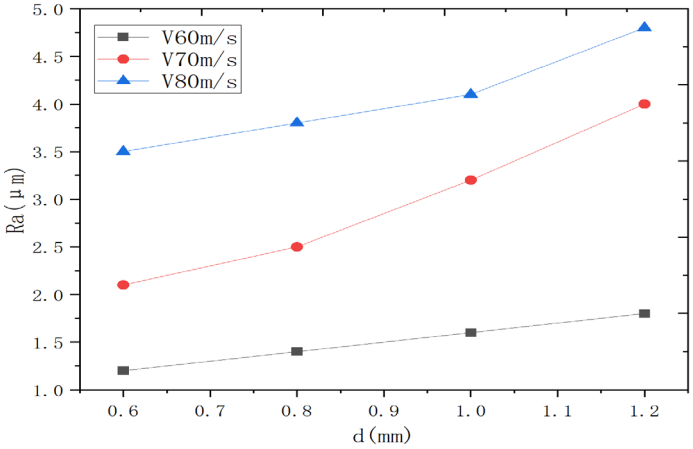

Fig. 9. Surface roughness of the substrate after slurry impact.

As shown in Fig. 9, with the increase of impact speed and abrasive particle size, the surface roughness of the matrix after impact increases. This indicates that as the impact energy of the slurry during the slurry throwing process increases, the degree of plastic deformation on the surface of the matrix increases, resulting in an increase in the depth of the wave valley. Therefore, the surface roughness increases. At the same time, it also indicates that when the abrasive particle size is less than 1mm, the impact speed has a greater impact on surface roughness than the abrasive particle size, When the abrasive particle size is greater than or equal to 1mm, the impact of abrasive particle size on surface roughness is higher than that of impact velocity.

Analysis of residual stress on the surface after slurry impact. Measure the residual stress on the surface of the substrate after impact using the IXRD residual stress tester. In order to accurately analyze the impact of slurry impact on residual stress on the substrate surface, this paper adopts a layered measurement of residual stress on the substrate surface. Firstly, the residual stress value on the 304 surface before the slurry experiment is tested. After the slurry impact, the sample is subjected to electrochemical polishing method, with a thickness of 10% μ Measure layer by layer in units of m until the test values are consistent with before the experiment, and this depth is the maximum depth. The experimental results are shown in Fig. 10.

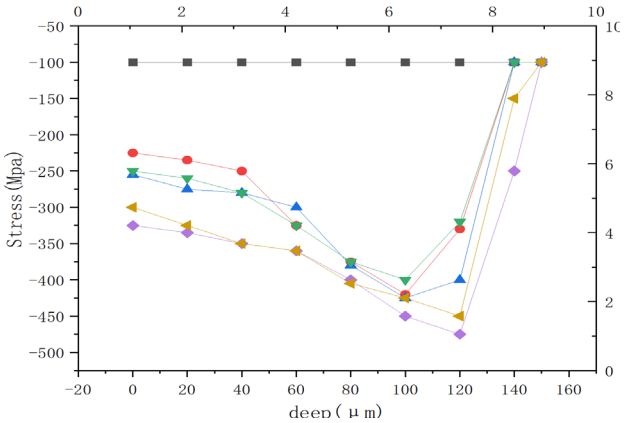

Fig. 10. Residual stress on the surface and depth of the substrate after slurry impact.

Fig. 10 shows that the maximum depth of residual stress after slurry impact is 120 μ M~140 μ m. And it shows a trend of first increasing and then decreasing, with the slope of the increasing process much lower than the decreasing slope, and the depth of the maximum residual stress is directly proportional to the impact energy. After slurry impact, a hardened layer is formed on the surface of the substrate due to residual stress, which improves surface strength and corrosion resistance, and improves service life to a certain extent. At the same time, the maximum depth of the hardened layer is 140 μ m. The impact on subsequent processes such as cold rolling and coating is minimal.

Analysis of surface corrosion resistance after slurry impact. Self corrosion current is a physical parameter that reflects electrochemical kinetics. The lower the corrosion current density, the stronger the corrosion resistance of the material; The self corrosion potential can indicate the tendency of a material to be corroded in a certain medium, and a larger or more positive value indicates that the material is less susceptible to corrosion [25]. In the anodic polarization zone, as the potential increases, the current density first increases exponentially. This curve represents the active dissolution zone, and the main reaction occurring in this stage is metal dissolution; Then the curve reaches a stage of gradual change. When the potential increases to a certain critical value, it reaches the passivation current density and passivation potential of the material. At this time, the current density will decrease or increase at an extremely slow rate with the increase of potential.

This is because as the voltage continues to scan towards the anode, a dense oxide film is formed on the surface of the substrate to protect it from corrosion or slow corrosion, This leads to passivation phenomenon. When the applied potential increases to a certain extent, the current density suddenly increases and continues to increase, and this potential is called the pitting potential. The oxide film of the sample is broken down by the applied voltage, resulting in pitting corrosion. The larger the pitting potential, the better the corrosion resistance of the material [26].

The electrochemical potentiodynamic polarization curves of unprocessed 304 stainless steel and samples after slurry impact are shown in Fig. 11.

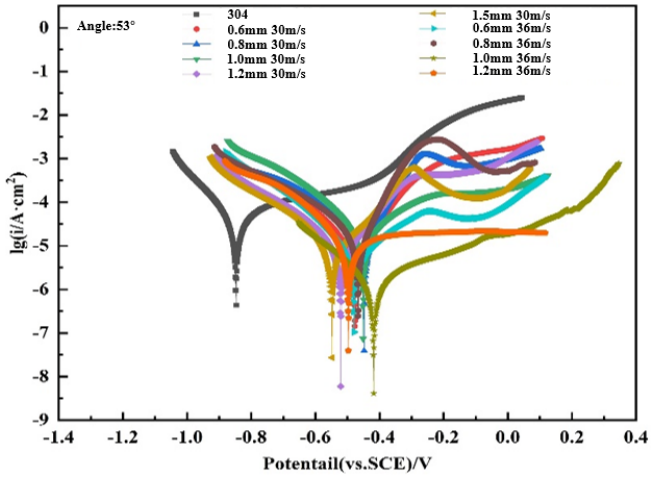

Fig. 11. Polarization curve after slurry impact.

From Fig.11, it can be seen that in the cathodic polarization zone, the corrosion current density on the surface of untreated 304 stainless steel substrate decreases sharply with the increase of potential. When the potential increases to -0.827 V, the current density increases again with the increase of potential. At this point, it enters the anodic polarization zone, and the intersection of the two curves at the junction of the anodic and cathodic polarization zones is the self corrosion potential value, which is approximately -0.827 V for the original sample. After slurry impact, the samples showed a corrected self corrosion potential compared to the original 304 stainless steel, indicating that the original 304 stainless steel had a higher corrosion tendency and faster corrosion rate during the activation stage. After slurry impact, the corrosion current density of the sample significantly decreased, with higher pitting potential and significantly enhanced passivation ability. The results indicate that the corrosion resistance of the substrate surface has significantly changed under the action of slurry impact energy after slurry impact.

Microscopic organization analysis. The metallographic diagram of the cross-section of the unprocessed sample and the matrix after slurry impact is shown in Fig. 12. From Fig. 12(a), it can be seen that the microstructure of 304 stainless steel is single-phase austenite, with clear and complete grain boundaries. The grains are basically equiaxed, and the grain size is relatively uniform, with a small amount of twinning structure present. Fig. 12(b) shows that after slurry impact, there is a clearly uncorroded black area at the boundary of the cross-section, which has not completely corroded within the same time, indicating a significant improvement in the corrosion resistance of the substrate surface after slurry impact.

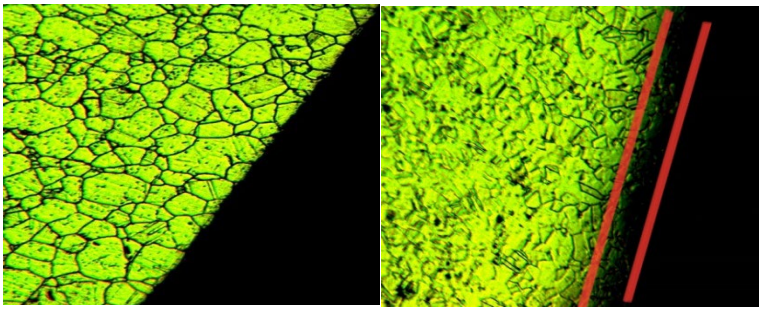

(a) Original section boundary （b） Boundary of cross-section after slurry throwing

Fig. 12. Crystal image before and after slurry throwing.

The IPF diagram of the EBSD test results is shown in Fig. 13(a), where it can be observed that the color representing the orientation within each grain of the original sample is relatively uniform. After slurry treatment, the results of the sample are shown in Fig. 13(b), where it can be seen that there is a clear preferred orientation of the grains on the surface of the matrix towards the<001>crystal plane.

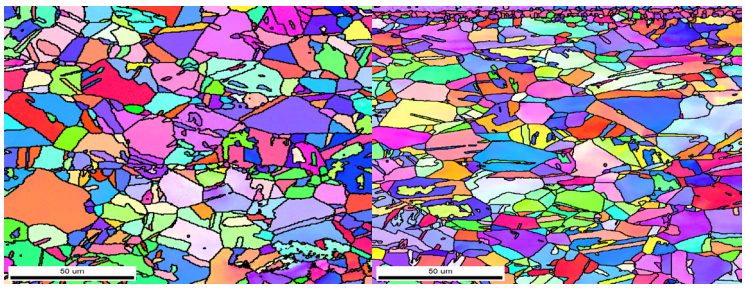

Fig. 13. IPF diagram of the EBSD.

The grain distribution of EBSD is shown in Fig. 14, and it can be seen from Fig. 14 that the grains on the surface layer of the matrix have undergone significant refinement after slurry treatment. Fig. 14(a) shows the original grain size, which can be seen to be mainly concentrated in the range of 10-30 μ Approximately m, with a maximum size of 41 μ m. Its average grain size is 24.03 μ M; The grain size diagram after slurry impact is shown in Fig. 14(b), with grains concentrated in 4-19 μ About m, maximum 22 μ m. The average grain size is 10.79 μ M. After the slurry impact, a large amount of twin structures were generated at the top of the matrix, which is due to the elastic-plastic deformation of the matrix and the formation of coherent twin boundaries. This twin boundary is a completely undistorted coherent crystal plane with low interfacial energy (about 1/10 of that of ordinary grain boundaries) and is very stable. They divide the original austenite grains into a large number of submicron small pieces, which have higher grain boundary density. This can promote the diffusion of Cr to the material surface and form a uniform and dense passivation film rich in Cr, reducing the contact area with the corrosive medium, preventing further erosion of the corrosive medium, and thus improving the corrosion resistance of the material.

Materials Research Proceedings 44 (2024) 167-181 https://doi.org/10.21741/9781644903254-19

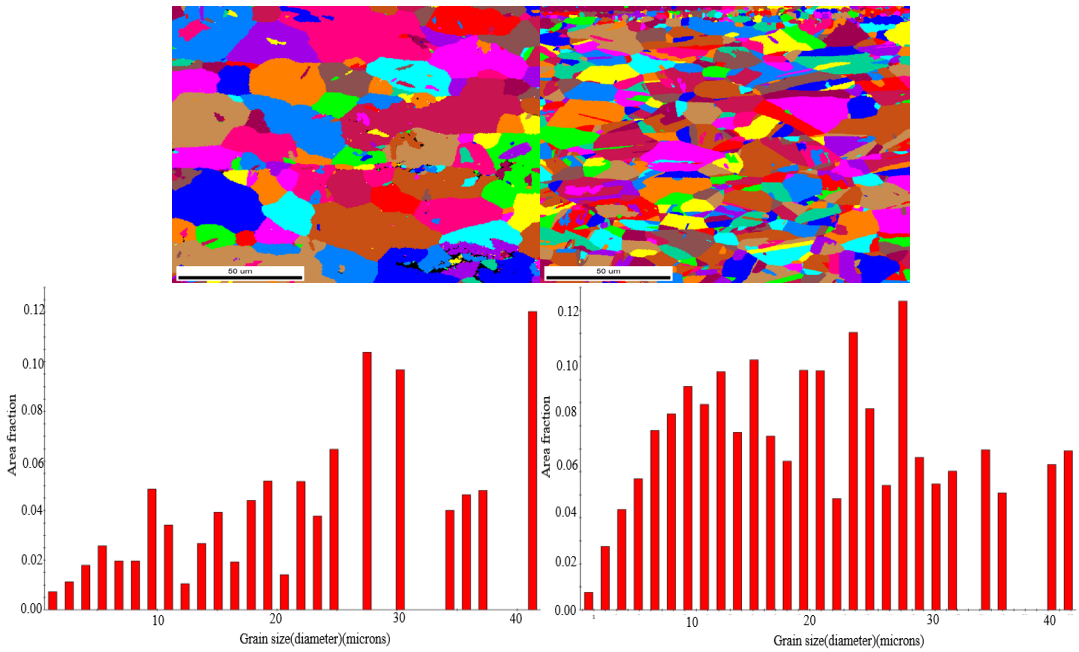

Fig. 14. Grain size of the EBSD.

The EBSD phase transition diagram is shown in Fig. 15, where the red area represents martensite and the green area represents austenite. Fig. 15(a) shows that there is only a single austenite phase in the matrix of the unprocessed 304 stainless steel sample. Fig. 15(b) shows that after slurry impact, a large amount of austenite transforms into martensite in the grains, with a martensite content of 9.8%. During the process of slurry impact, 304 stainless steel undergoes elastic-plastic deformation on the surface layer of the matrix under continuous impact of the slurry. The deformation energy provides a certain amount of energy for the phase transformation, achieving the minimum driving force required for martensitic transformation. Austenitic transformation induces martensitic transformation, which is mainly distributed at the austenite grain boundaries. The generation of martensite reduces the distance between austenite grain boundaries and improves the density of crystals. Therefore, the difficulty of ions entering the grain boundaries increases, thereby improving the corrosion resistance of the matrix surface.

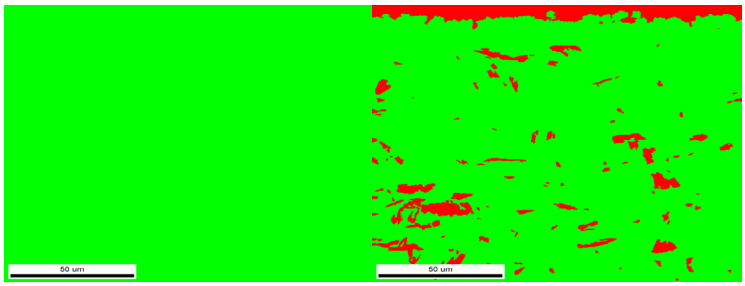

Fig. 15. EBSD phase transition diagram.

After slurry impact, the surface of the matrix undergoes elastic-plastic deformation, and the deformation reflected in the microstructure is dominated by dislocation slip. As shown in Fig. 16, the dislocation density significantly increases in the refined area of the substrate surface, and the intersection between dislocations will increase. This will lead to an increase in dislocation slip resistance, which to some extent prevents the slip of the crystal structure, ensures the stability of the crystal, delays the corrosion rate, and improves the corrosion resistance of the substrate.

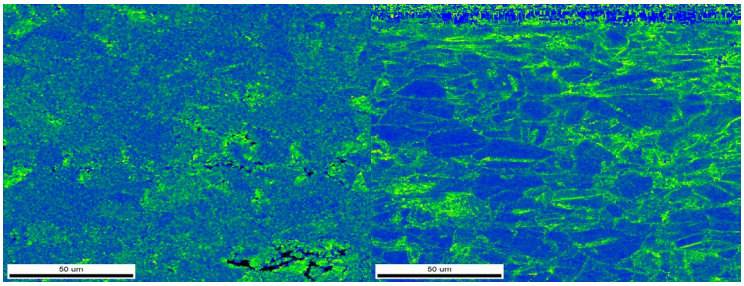

Fig. 16. EBSD dislocation density significantly.

The unprocessed grain boundary diagram of 304 stainless steel is shown in Fig. 17(a), and the grain boundary diagram after slurry treatment is shown in Fig. 17(b).

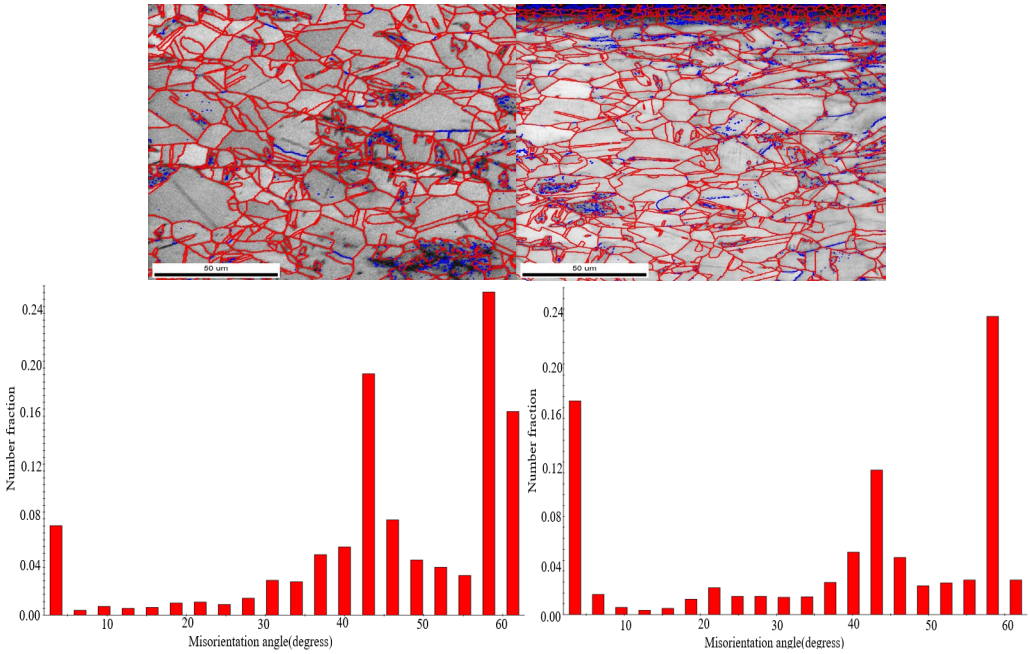

Fig. 17. EBSD grain boundary diagram.

The blue boundary represents small angle grain boundaries (with a phase difference of 2 °~10 °), and the red boundary represents large angle grain boundaries (with a phase difference greater than 10 °). The content of small angle grain boundaries in the original board is only 7.3%, while after slurry treatment, a large amount of small angle grain boundaries with a content of 21.9% are generated on the surface of the matrix. From the statistical chart, it can be seen that the original sheet is mainly composed of high angle grain boundaries, mainly concentrated at 40 °~60 °, with an average orientation difference of 45.52 °; After slurry treatment, there is a significant increase in small angle grain boundaries in the board, mainly concentrated at around 5 °, with an average orientation difference of 37.89 °. The energy of small angle grain boundaries is lower and more stable, resulting in better corrosion resistance.

Conclusions

This article analyzes the mechanism of elastic-plastic deformation on the surface of 304 stainless steel substrate under slurry impact, simulates the slurry process using finite element software, and finally conducts slurry impact tests to analyze the surface integrity of the 304 stainless steel substrate after impact. The conclusions are as follows：

（1） The maximum temperature on the substrate surface under different abrasive particle sizes, blasting speeds, and blasting angles is 95 ℃，When other process parameters

are the same, the impact range and depth of the substrate surface after slurry blast will increase with the increase of abrasive particle size and injection speed. As the blasting angle increases, the impact depth will show a trend of increasing, and the blast range will show a trend of first increasing and then decreasing with the increase of ejection angle. When the ejection angle is 75 °,the blast range is the largest. When other process parameters are the same and the abrasive particle size increases.

（2） The surface roughness value of the metal substrate after slurry impact increases with the increase of abrasive particle size, and the difference between the surface roughness after impact gradually increases with the increase of abrasive particle size; The residual stress on the substrate surface after slurry impact will increase with the increase of abrasive particle size, blast speed, and blast angle; The maximum hardened layer after slurry impact is 140 μm. The residual stress shows a trend of first increasing and then decreasing with the depth of the layer. The minimum corrosion current density on the substrate surface after slurry impact can reach $1.29*10^{-6}A/cm^2$, the corrosion resistance of the substrate surface has been significantly improved, and the EBSD results show that the grains after slurry impact are concentrated in 4-19 μm About m, maximum 22 μm. The average grain size is 10.79 μm.

Reference

[1] K. Voges, A. Mueth, Eco-pickled surface：an environmentally advantageous alternative to conventional acid pickling, Iron Steel Technol. 4 (2008) 81-96.

[2] J.G.A. Bitter, A study of erosion phenomena: Part I, Wear 6 (1963) 5-21. https://doi.org/10.1016/0043-1648(63)90003-6

[3] J.G.A. Bitter, A study of erosion phenomena: Part II, Wear 6 (1963) 169-190. https://doi.org/10.1016/0043-1648(63)90073-5

[4] C. Zhang, Y. Zhang, F. Zhang, D. Luan, Study on Removal Model of Abrasive Waterjet Machining, J. Mech. Eng. 51 (2015) 188-196. https://doi.org/10.3901/JME.2015.07.188

[5] J. Li, A. Du, Y. Fan, X. Zhao, R. Ma, J. Wu, Effect of shot-blasting pretreatment on microstructures of hot-dip galvanized coating, Surf. Coat. Tech. 4 (20190 218-224. https://doi.org/10.1016/j.surfcoat.2019.02.075

[6] Ramprasad, G. Upadhyay, K. Hassan, Optimization MRR Of stainless steel 403 in abrasive water jet machining using Anova and Taguchi method, Int. J. Eng. Res. Appl. 5 (2015) 86-91.

[7] K. Voges, A. Mueth, Eco-pickled surface：an environmentally advantageous alternative to conventional acid pickling, Iron Steel Technol. 4 (2008) 81-96.

[8] C. Fengjun, A review of research on abrasive jet surface polishing, Surf. Technol. 44 (2015) 119-123. https://doi.org/10.16490/j.cnki.issn.1001-3660.2015.11.019

[9] V. Chaturvedi, D. Singh, Mutli Response optimization of process parameters of abrasive water jet machining for stainless steel AISI 304 using VIKOR approach coupled with signal to noise ratio mechnology, J. Adv. Manuf. Syst. 14 (2015) 107-121. https://doi.org/10.1142/S0219686715500080

[10] S.R. Lohar, P.R. Kubade. Current research and development in abrasive water jet machining (AWJM): A Review, Int. J. Sci. Res. 5 (2016) 996-999.

[11] B. Levy, M. EI Mansori, M. El Hadrouz, S. Mezghani, A.-L. Beaudonnet, J. Cabrero, Smart tribo-peening process for surface functionalization through digital twin concept, Adv. Manuf. Technol. 4 (2021) 1-23. https://doi.org/10.1007/s00170-021-07143-x

[12] N. Minhas, A. Thakur, S. Mehlwal, Multi-variable Optimization of the Shot Blasting of Additively Manufactured AlSi10Mg Plates for Surface Roughness Using Response Surface Methodology, Arabian J. Sci. Eng. 4 (2021) 1-15.

[13] Z. Li, F. Yang, Y. Liu, Y. Gao, Numerical Simulation of Derusting Treatment of Steel Parts By Shot Blast, CMES 120 (2019) 486-500. https://doi.org/10.32604/cmes.2019.05187

[14] P. Moonchaleanporn, S. Songkuea, J. Klanpolrang, P. Payaksak, K. Wongpinkaew, N. Bunchoo, E. Viyanit, A. Manonukul, Improving corrosion resistance in sintered 304L stainless steel using shot blasting, Int. J. Mater. Product Technol. 59 (2019) 172-191. https://doi.org/10.1504/IJMPT.2019.102643

[15] G. Singh, S. Singh, C. Prakash, S. Ramakrishna, On investigating the soda-lime shot blasting of AZ31 alloy: Effects on surface roughness, material removal rate, corrosion resistance, and bioactivity, J. Magnesium Alloy. 9 (2021) 1272-1284. https://doi.org/10.1016/j.jma.2020.11.017

[16] U. Oberste-Lehn, C. Beamer, P. Gümpel, A. Karl, Corrosion resistance of low-temperature, surface-hardened stainless steel, Mater. Perform. 58 (2019) 42-46.

[17] X. Zhang, Mechanism and Experimental Study on Surface Oxidation Skin Rupture of Q235 Strip Steel, Taiyuan University of science and technology, 2016.

[18] D. Bian, Research on the critical fracture stress of Q235 oxide scale, Taiyuan University of science and technology, 2013.

[19] M. Parsi, K. Najmi, F. Najafifard, S. Hassani, B.S. McLaury, S.A. Shirazi, A comprehensive review of solid particle erosion modeling for oil and gas wells and pipelines applications, J. Natural Gas Sci. Eng. 21 (2014) 850-873. https://doi.org/10.1016/j.jngse.2014.10.001

[20] S. Wang, Simulation and Experimental Study on Shot Blasting Impact Process for Acid Free Descaling of Rolled Strip Steel, Beijing: University of Science and Technology Beijing, 2018.

[21] L. Zhai, Mechanism, Evaluation and Application of Shot Blasting Strengthening, Heat Treat. Tech. Equip. 29 (2008) 53-66.

[22] F. Chen, W. Ge, Review of smooth particle hydrodynamics methods for multiphase flow, J. Mech 53 (2021) 1-17.

[23] W.B. Rowe, M.N. Morgan, S.C.E. Black, B. Mills, A simplified approach to control of thermal damage in grinding, CIRP annals 45 (1996) 299-302. https://doi.org/10.1016/S0007-8506(07)63067-4

[24] Z. Yu, Study on the influence of shape and position characteristics of abrasive particles and their proportions on the thermodynamic coupling process of grinding, Liaoning: Northeastern University, 2019.

[25] H. Yang, Study on Preparation and Properties of Sol gel Anticorrosive Coating on Aluminum Alloy, Xi'an University of technology, 2021.

[26] Y. Wang, Overview of research on pitting corrosion of stainless steel, Corros. Sci. Protect. Tech. 27 (2015) 387-392.